

Article

Experimental and CFD Modelling: Impact of the Inlet Slug Flow on the Horizontal Gas–Liquid Separator

Siong Hoong Lee ^{1,*}, Thomas S. Y. Choong ^{1,*}, Luqman Chuah Abdullah ¹,
Mus'ab Abdul Razak ¹ and Zhen Hong Ban ^{2,3}

¹ Department of Chemical and Environmental Engineering/Sustainable Process Engineering Research Center (SPERC), Universiti Putra Malaysia, 43400 UPM Serdang, Selangor, Malaysia; chuah@upm.edu.my (L.C.A.); musab@upm.edu.my (M.A.R.)

² School of Energy and Chemical Engineering, Xiamen University Malaysia, 43900 Sepang, Selangor, Malaysia; bzhong@xmu.edu.my

³ College of Chemistry and Chemical Engineering, Xiamen University, 361005 Xiamen, China

* Correspondence: leesiohng@yaho.com (S.H.L.); csthomas@upm.edu.my (T.S.Y.C.); Tel.: +603-89466293 (S.H.L.)

Received: 11 October 2018; Accepted: 5 November 2018; Published: 24 December 2018



Abstract: For a gas-liquid separator sizing, many engineers have neglected the flow pattern of incoming fluids. The impact of inlet slug flow which impeded onto the separator's liquid phase will cause a separator fails to perform when sloshing happened in the separator. To date, the study on verifying the impact of inlet slug flow in a separator remains limited. In this paper, the impact of inlet momentum and inlet slug flow on the hydrodynamics in a separator for cases without an inlet device were investigated. The experimental and Computational Fluid Dynamics (CFD) results of cavity formation and sloshing occurrence in the separator in this study were compared. A User Defined Function (UDF) was used to describe the inlet slug flow at the separator inlet. Inlet slug flow occurred at inlet momentum from 200 to 1000 Pa, and sloshing occurred in the separator at 1000 Pa. Both experimental and simulated results showed similar phenomena.

Keywords: gas-liquid separator; inlet slug flow; cavity formation; sloshing; Computational Fluid Dynamics (CFD)

1. Introduction

A two-phase or gas-liquid separator is commonly used in oil and gas production. A gas-liquid separator is a cylindrical vessel equipped with a liquid level control where the upper part is a gas-filled compartment, and the lower part is a liquid-filled compartment. The main function of a gas-liquid separator is for bulk phase separation, control, or dissipation the energy of the fluids as they leave the flowline and enter the separator [1,2].

To ensure the performance of a separator, Hansen (2001) has proposed several important general criteria, i.e., (1) to provide sufficient time to allow the immiscible gas and liquid phases to separate by gravity, (2) to provide sufficient time to allow for the coalescence of gas bubbles to improve degassing, (3) to allow for variation in the flow rates of gas and liquid or simply known as inlet momentum into the separator without adversely affecting separation efficiency [2]. These three criteria are important to ensure the gas and liquid can be separated into two distinct phases in the separator. The inlet momentum of incoming fluids is calculated based on mixture density, ρ_m (kg/m³) multiply with square of mixture mean volume flow velocity, v_m^2 (m/s) in the flowlines, as shown in Equation (1).

$$\text{Inlet Momentum} = \rho_m v_m^2 \quad (1)$$

Based on current industrial practice, the inlet momentum will determine the type of inlet device that is used in a separator. An inlet device is one of the tools that is commonly used to control the incoming flow distribution in a gas–liquid separator. This device is installed at the inlet section of a separator, in order to pre-separate the gas and liquid phase, and to reduce the momentum in the separator.

The recommendation of an inlet device based on inlet momentum, which is currently practised in the industries, is summarized in Table 1 [3].

Table 1. Recommended inlet device according to inlet momentum limit [3].

Type of Inlet Device	Inlet Momentum, kg/ms ² or Pa or N/m ²
No Inlet Device	1043
Diverter Plate	1415
Half Open Pipe	2085
Inlet Vane	8043
Inlet Cyclone	14,895

The calculated inlet momentum based on Equation (1) is represented by the average value of the incoming flow entering a separator. The gas and liquid flowrate fluctuation in the incoming flow due to its flow pattern are not considered. Therefore, inlet slug flow was studied to demonstrate the impact of incoming flow pattern in the separator in this study.

Inlet slug flow was selected due to reports of some researchers, such as Chin (2015) and Miyoshi et al. (1988), who highlighted that occurrence of excessive liquid carryover at gas outlet of a separator. The investigation shall be conducted for inlet slug flow which caused high liquid carryover although demister was installed in the separator. This inlet slug flow also causes mechanical damages in the separator [4,5]. The slug flow pattern can be described as a stratified flow with intermittent appearance of aerated liquid slugs travelling at high velocity. This aerated liquid slugs phenomena was described as hydraulic jump by Vallee et al. (2010) in their study [6]. The occurrence of hydraulic jump in the slug flow will increase with increment of gas flowrate [7]. During the hydraulic jump, the travelling force of the flow will increase due to drastic changes in liquid volume fraction. Therefore, as mentioned by Bonzanini et al. (2018) and Wai et al. (2016), the impact pressure of slug flow is much higher than stratified flow due to higher fluids velocity in the slug flow [8,9]. In most cases, hydraulic jump in the slug flow was formed in the pipeline before entering a gas–liquid separator. The impact of hydraulic jump in the slug flow onto the liquid in the separator which might cause severe turbulent in the separator is still remains unknown. Hence, the impact of the inlet flow pattern is often neglected during separator sizing, and the process engineer will follow the general guideline by the industry standard [3,10].

In this work, hydrodynamics in a separator with inlet slug flow was studied. The separator was sized, based on industry practised guidelines. The study was conducted in two stages; the first stage included experimental works where the impact of an inlet slug flow onto the liquid surface in a separator. Furthermore, the hydrodynamics in the separator was observed and recorded. While in second stage, Computational Fluid Dynamics (CFD) was used to simulate the hydrodynamics in the separator including liquid turbulence in the separator which impeded by the incoming gas–liquid mixture. The developed CFD model is expected to provide insights in the separator performance, with slug flow as the inlet condition.

2. Experimental Work

2.1. Experimental Methodology

In the first stage, experimental works were carried out to study the impact of inlet slug flow and the turbulence in the separator. Five cases with inlet momentums of 200, 400, 600, 800, and 1000 Pa were investigated. The mass flow rate of incoming liquid was fixed at 0.00702 kg/s for all the cases. The mass flow rate of the gas was manipulated in the range from 0.00007 kg/s to 0.000342 kg/s, in order to match the particular inlet momentum.

Experimental Setup

The experiment was conducted using an atmospheric pressure air–water separation test rig with a horizontal gas–liquid separator made from Schedule 40 of 3-inch transparent Polyvinyl Chloride (PVC) with an internal diameter of 77.928 mm and an total length of 312 mm, which was sized according to an industrial standard. At testing inlet momentum, the gas phase constant is less than 0.7 m/s, and a demister is not required in the separator [3]. The liquid level inside the separator was controlled at 66 mm from the bottom of the test separator, which provided a retention time of 3 min as suggested by American Petroleum Institute (API) standard [10]. At this height, the water occupied about 84.7% of the separator height. The internal diameter of the separator inlet was 7.747 mm. The separator was illustrated in Figure 1.

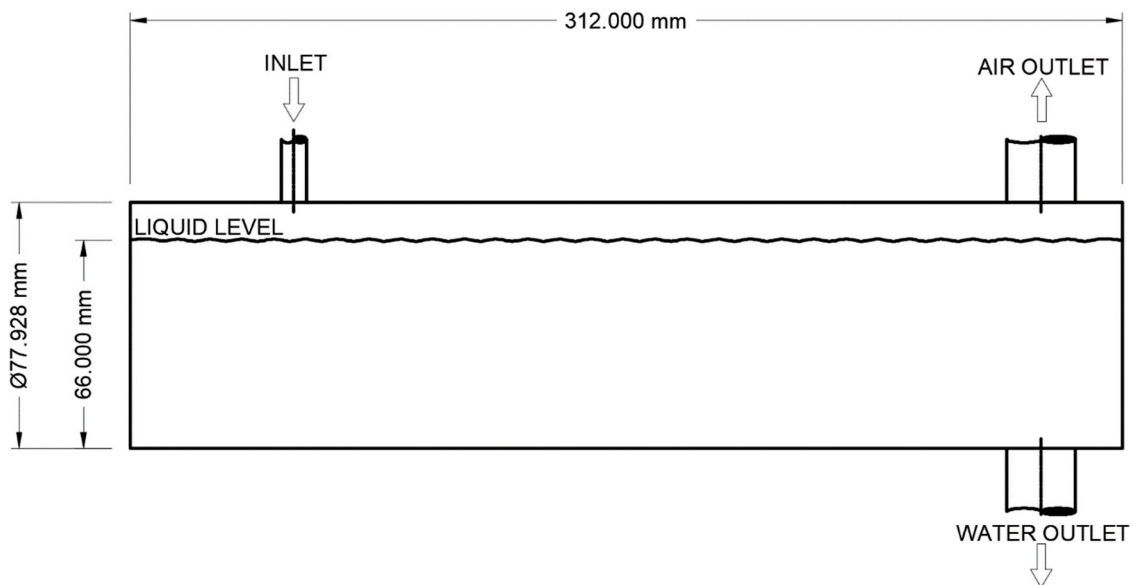


Figure 1. Sketch of the separator and its dimension used in the experiment.

During the experiment, liquid was fed into the system using a peristaltic pump. Once the required liquid level in the test separator was achieved, gas from compressor was slowly introduced into the system. The gas flowrate was regulated and measured using a valve incorporated in the flowmeter. Once the required gas flowrate based on inlet momentum was achieved, the system was left for stabilization. A video camera (PowerShot A2500, Canon (China) Co. Ltd., Beijing, China) was setup to record the movement of gas and liquid inside the separator. The medium used in this testing were air and water as gas, and liquid phase respectively. Figure 2 shows the set-up of the atmospheric pressure test rig.

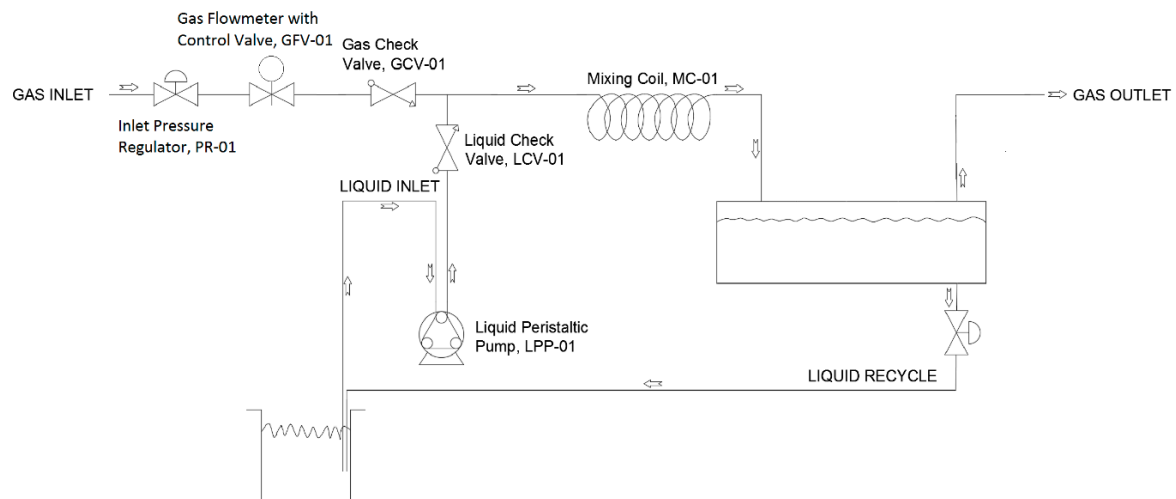


Figure 2. A schematic diagram of test rig.

2.2. Result and Discussion of Experimental Work

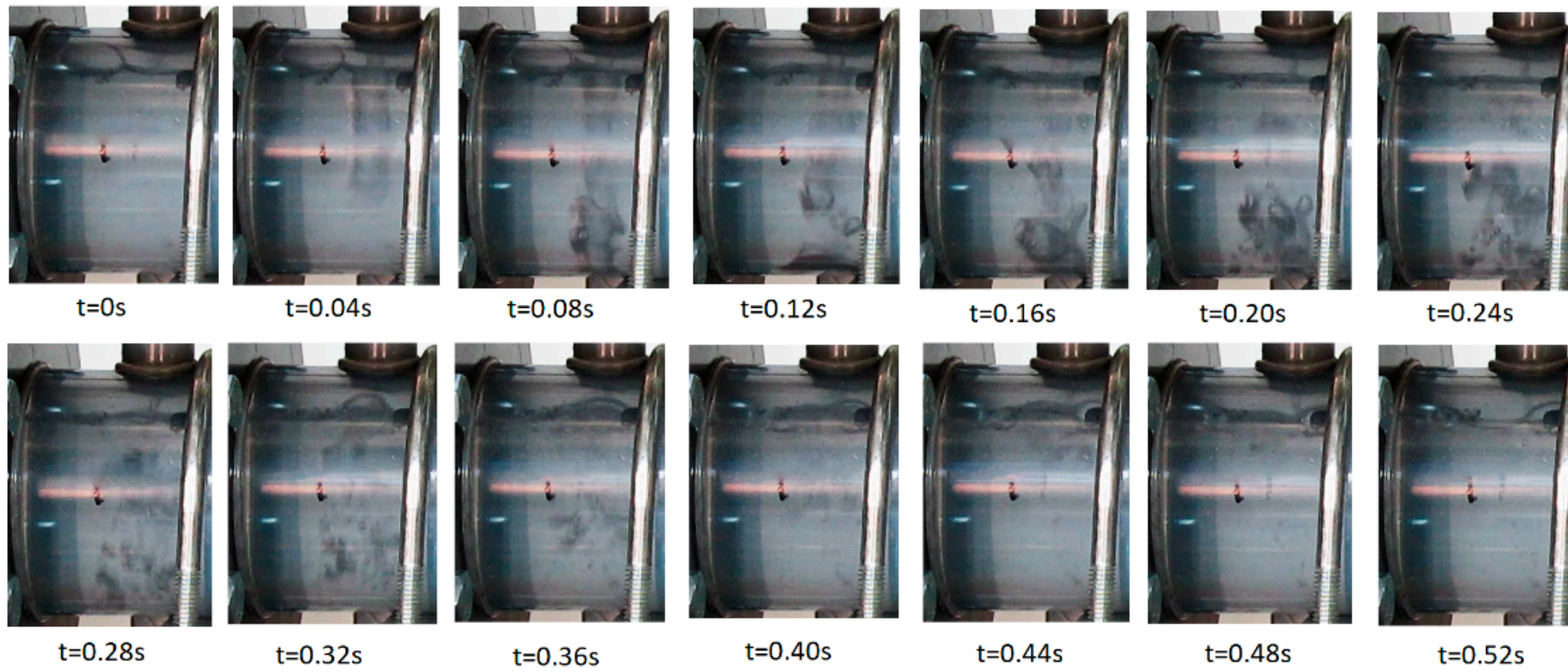
2.2.1. Cavity Formation

Cavity formation in the liquid was observed in all the five cases studied in current work. Cavity was described as depression on the liquid surface caused by the impingement of incoming jet [11,12]. This observation was the main focus in current work as the cavity has caused more turbulence, and both gas and liquid were not flowing at calm stratified flow condition in the separator. The turbulence in the separator might increase the liquid carryover from the separator.

Figure 3a–e show cavity formation in the separator at different inlet momentum. The inlet gas–liquid flow was found to enter the separator in the form of an intermittent pulsing jet flow, where a peak flow was observed at the inlet. This created a deep cavity in the liquid inside the separator. Before and after the pulsing jet, the impact of the incoming flow was much lesser and almost negligible for an inlet of momentum 600 Pa and below. For an inlet momentum of 800 Pa and above, the liquid in the separator were disturbed more greatly by the inlet flow, even after the peak flow. The maximum cavity observed in the experiment for inlet momentum of 200, 400, 600, 800, and 1000 Pa was at 0.08, 0.04, 0.12, 0.04, and 0.16 s respectively.

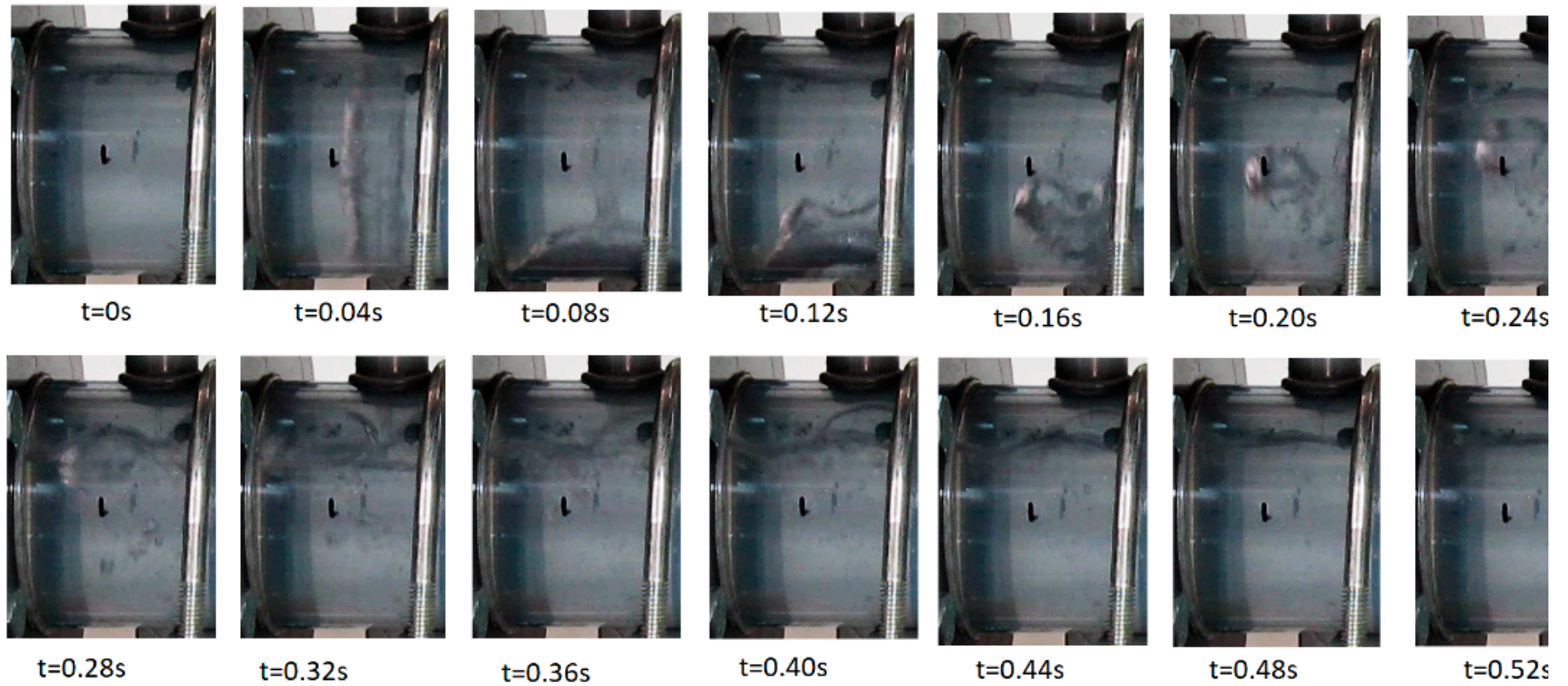
From the experiment observation, the cavity was most likely formed by the hitting of hydraulic jump of the inlet slug flow from the inlet onto the water surface. This observation has further confirmed that the hydraulic jump has formed in the pipeline, transferring the gas and liquid before entering the separator. The liquid fraction in the pipeline accumulated, and became a larger volume with a higher mass that would form a larger cavity in the liquid. Thus, a sudden spike of inlet momentum could be observed at the time when the inlet slug flow hit the liquid. This phenomenon was analyzed in detail in Section 3.2.1 with the aid of CFD results.

In addition, the flow condition in the pipeline transferring gas and liquid into the separator was predicted using the Mandhane's flow map, as shown in Figure 4 [13]. Mandhane's map predicted the slug flow as the flow pattern for an inlet momentum from 200 to 1000 Pa. Therefore, the cavity was mostly generated by the hydraulic jump of the inlet slug flow formed in the pipeline.



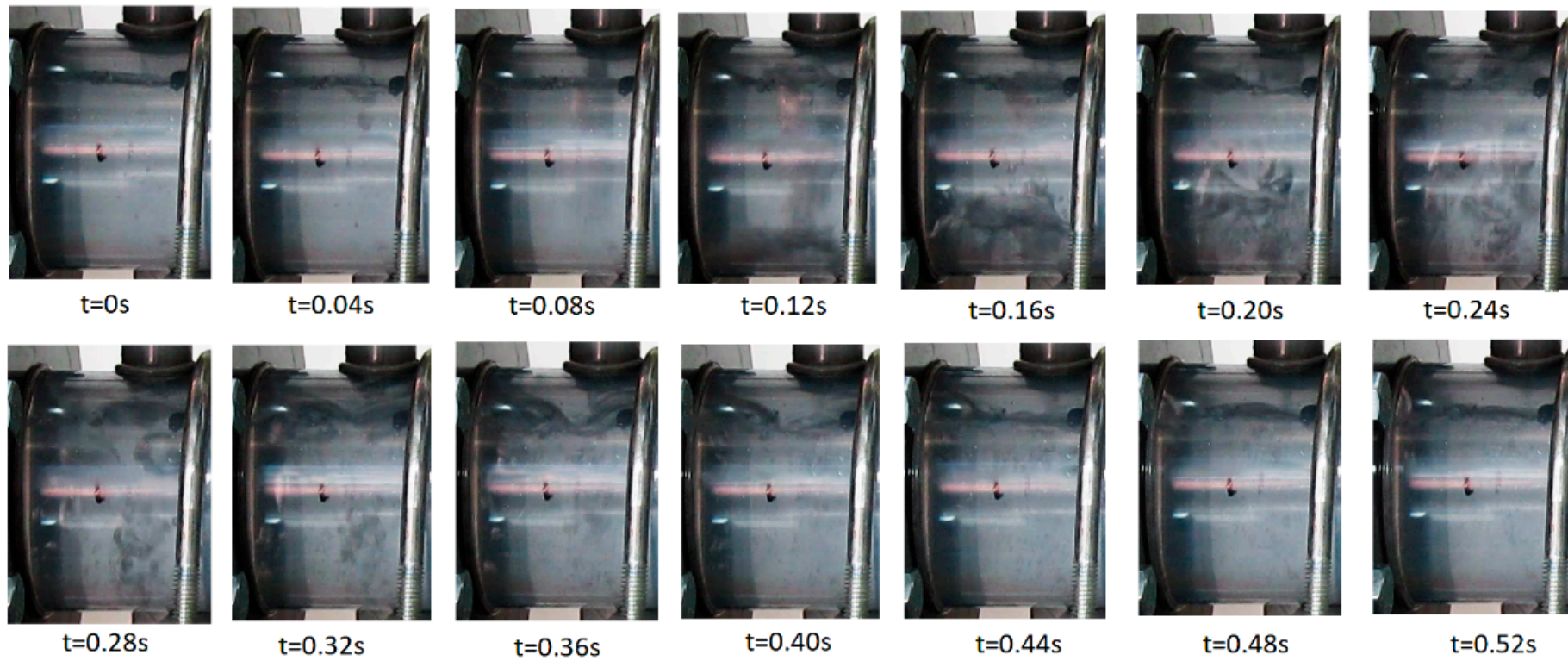
(a)

Figure 3. Cont.



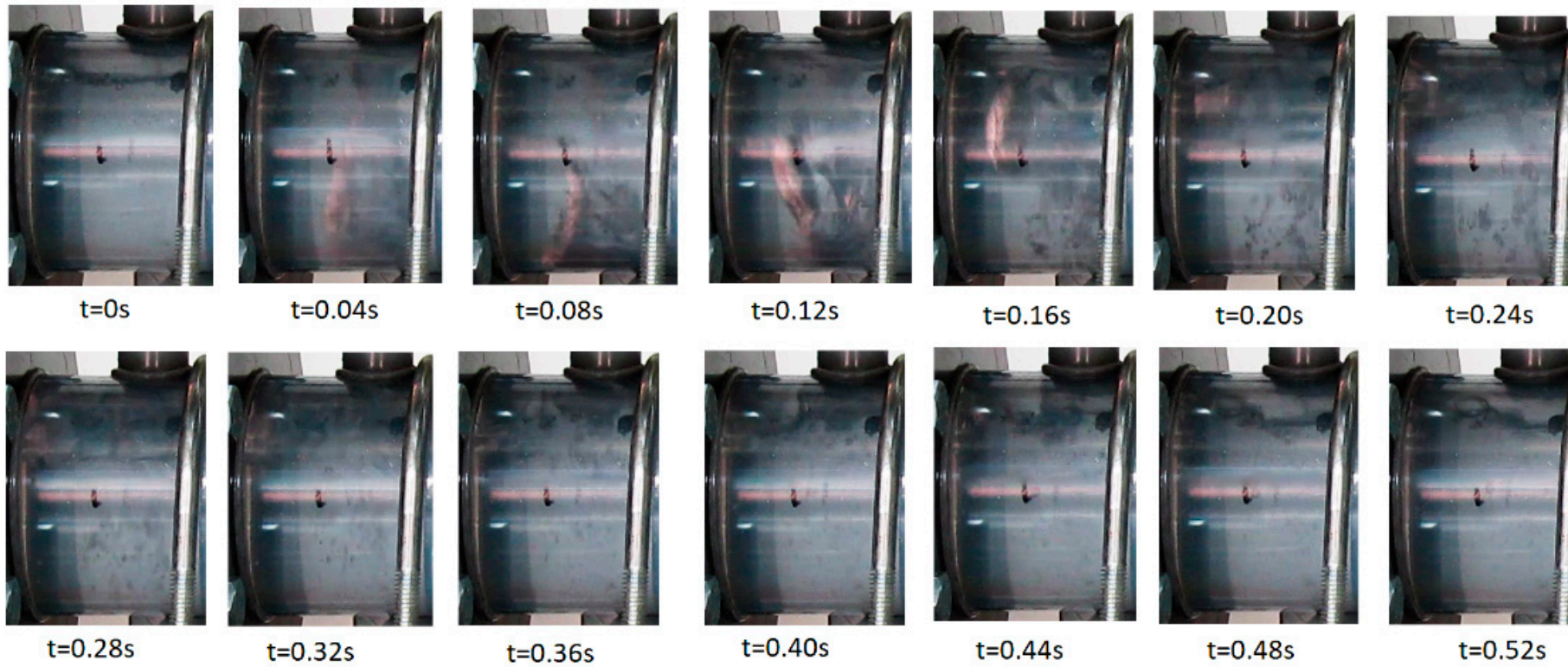
(b)

Figure 3. Cont.



(c)

Figure 3. Cont.



(d)

Figure 3. Cont.

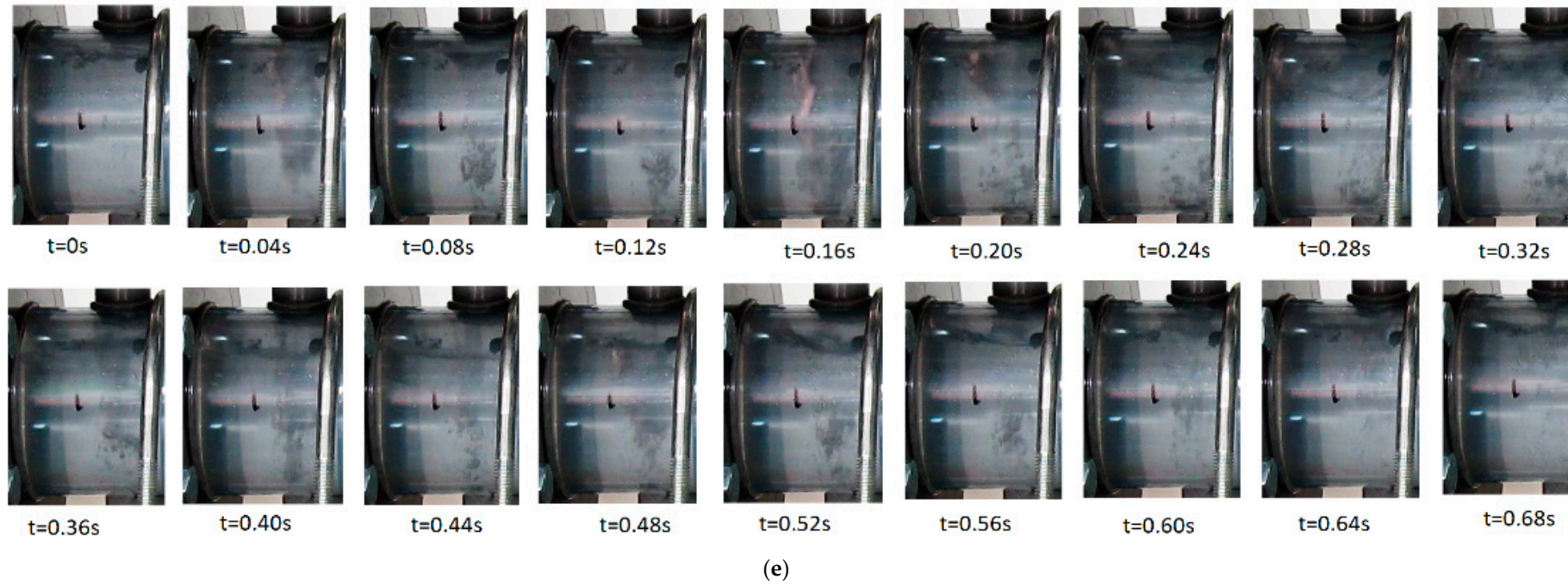


Figure 3. (a) Cavity formation at an inlet momentum of 200 Pa; (b) Cavity formation at an inlet momentum of 400 Pa; (c) Cavity formation at an inlet momentum of 600 Pa; (d) Cavity formation at an inlet momentum of 800 Pa; (e) Cavity formation at an inlet momentum of 1000 Pa.

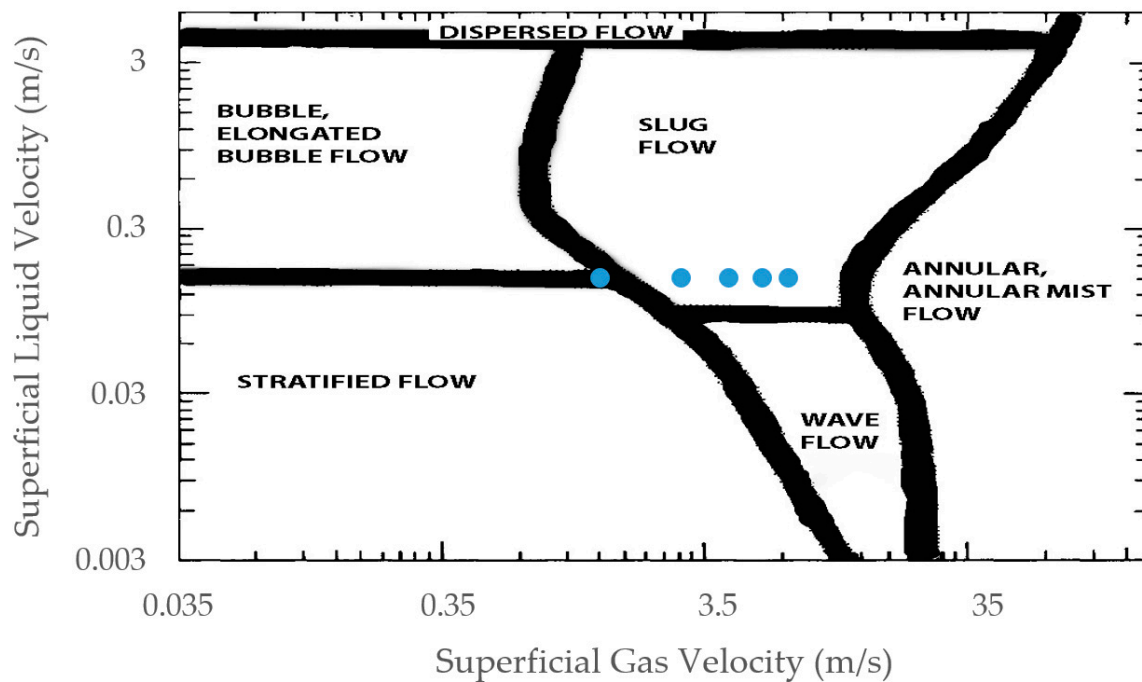


Figure 4. Flow pattern map adapted from Mandhane et al. (1974) [13].

2.2.2. Hydrodynamics in Separator

Figure 5a–e show the flow profile in the separator after the hydraulic jump, as observed in the experiment. The liquid surface inside the separator was found to be greatly disturbed by the impact of the inlet slug flow. For an inlet momentum of 200 Pa, after the peak flow where a cavity was formed in the liquid, a weak wave was generated along the separator. The wave intensity increased as the inlet momentum increased. Instead of a perfect stratified flow, a wavy stratified flow was observed inside the separator, for cases with an inlet momentum of 200 to 800 Pa. For an inlet momentum of 1000 Pa, the inlet slug flow created sloshing inside the separator. From the observation, the wave intensity was mainly affected by the volume of gas in the cavity caused by the inlet slug flow. At a higher inlet momentum, the cavity was filled with more gas. For a low inlet momentum (200 to 600 Pa), the cavity was filled with a mixture of gas and liquid, and only a weak wave was generated from the impact. At an inlet momentum of 800 Pa, a stronger gas pocket was generated, and it pushed the liquid aside and subsequently created a higher intensity wave along the separator length. For an inlet momentum of 1000 Pa, the intensity of the wave generated was strong enough to cause sloshing in the separator.

Figure 6 shows the hydrodynamics in the separator when sloshing occurred. Sloshing was found to occur only at an inlet momentum of 1000 Pa. This sloshing caused re-entrainment of liquid and pushed the liquid out via the separator gas outlet. A high amount of liquid was significantly pushed out from the separator during sloshing, and the amount of liquid carried over in the gas phase. Thus, sloshing was an unwanted condition occurring in the separator. The occurrence of sloshing was one of the important points to be highlighted in current work. The common industrial practice has recommended the use of no inlet device design for an inlet momentum of up to 1043 Pa, as discussed in Section 1. However, the findings in current work has shown that the separator might fail to work, even at an inlet momentum of 1000 Pa, if inlet slug flow occurred at the separator inlet. Therefore, extra precautions to check the inlet flow pattern are recommended, in order to ensure that the separator works.

Inlet Momentum (Pa)	t = 0.50 s	t = 0.62 s	t = 0.74 s
200			
			

(a)

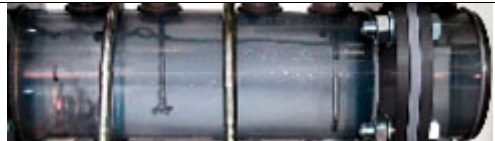
Inlet Momentum (Pa)	t = 0.50 s	t = 0.62 s	t = 0.74 s
400			
			

(b)

Figure 5. Cont.

Inlet Momentum (Pa)	t = 0.50 s	t = 0.62 s	t = 0.74 s
600			
			

(c)

Inlet Momentum (Pa)	t = 0.50 s	t = 0.62 s	t = 0.74 s
800			
			

(d)

Figure 5. Cont.

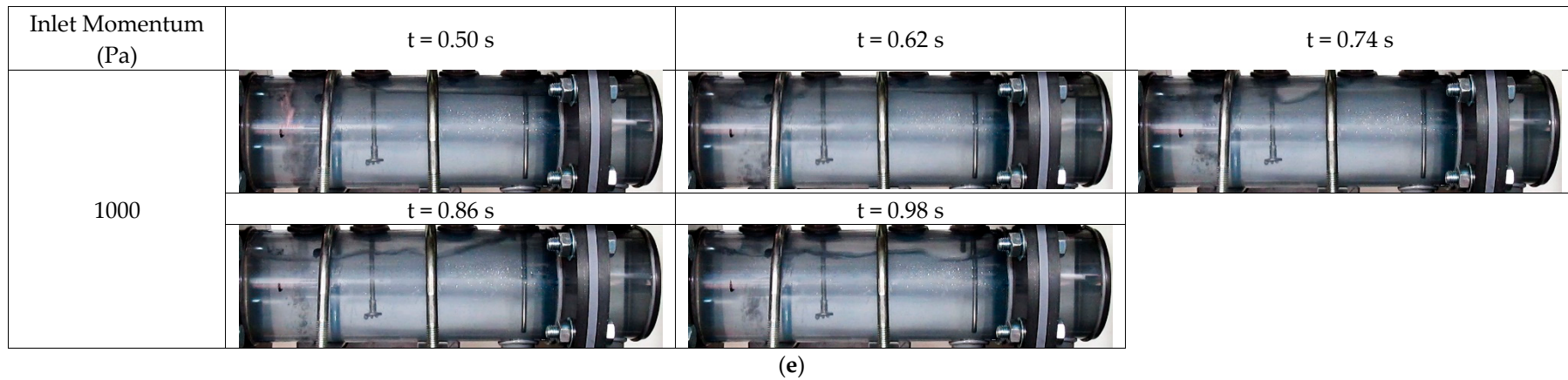


Figure 5. (a) Experimental observations for hydrodynamics inside the separator for 200 Pa; (b) Experiment observations for hydrodynamics inside the separator for 400 Pa; (c) Experimental observations for hydrodynamics inside the separator for 600 Pa; (d) Experiment observations for hydrodynamics inside the separator for 800 Pa; (e) Experiment observations for hydrodynamics inside the separator for 1000 Pa.

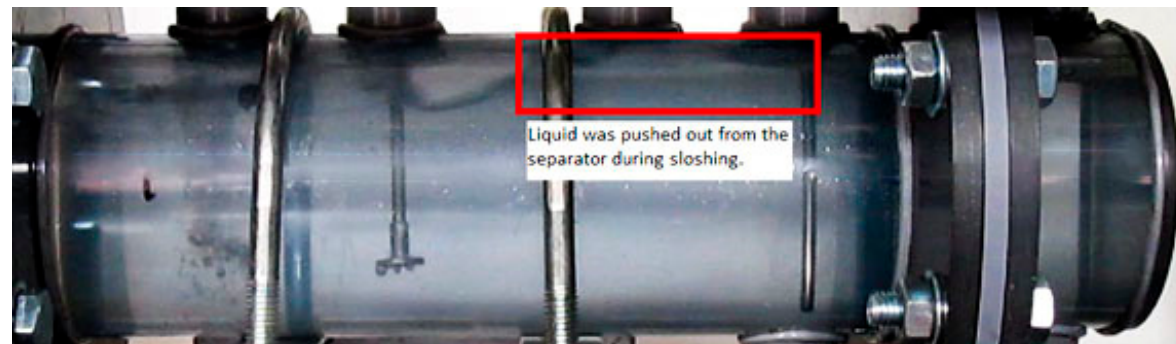


Figure 6. Sloshing in the Separator.

3. Computational Fluid Dynamics Work

3.1. Computational Fluid Dynamics Methodology

The CFD results were validated with the experimental works, and the hydrodynamics in the separator was further analyzed. Five cases with inlet momentums of 200, 400, 600, 800, and 1000 Pa were investigated for a duration of 1 s, with both experimental and CFD modelling approaches, as discussed in detail in Sections 3.1 and 3.2.

3.1.1. Computational Fluids Dynamics Setup

The CFD was used to simulate the inlet slug flow and hydrodynamics inside the separator in this study using commercial software, (Fluent 19, ANSYS Inc., Canonsburg, PA, USA). The Volume of Fluid (VOF) model was used due to this model is a surface-tracking technique applied to a fixed Eulerian mesh. It is designed for two or more immiscible fluids where the position of the interface between the fluids is of interest. VOF is commonly used by researchers to model stratified flow, two-phase flow, and free surface flow [14–16]. Meanwhile, the realizable k - ϵ turbulence model of Shih et al. (1995) [17] was selected in this study, due to its superior performance in jet flow and have proven by Ozan & Yüksel (2010) and Farzad & Hamed (2010) [18,19]. The separator model was meshed with tetrahedron with total cells of 477,294 with maximum skewness of 0.81369, as shown in Figure 7; the settings are shown in Table 2.

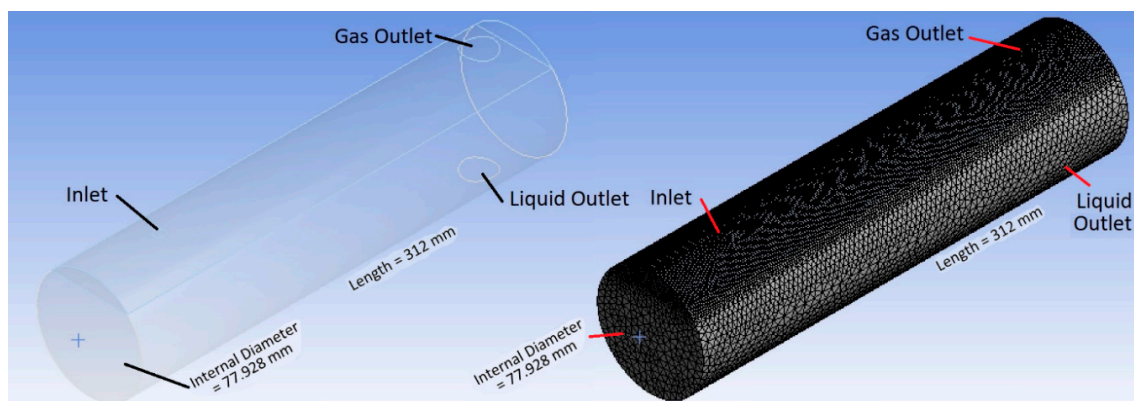


Figure 7. Separator model and separator with mesh.

Table 2. Computational fluid dynamics (CFD) settings for the separator.

Parameter	Description	Value or Settings
Quality of Mesh	Skewness	Max: 0.81369 Average: 0.22268
Discretization Scheme	Gradient Pressure Momentum Volume Fraction Turbulent Kinetic Energy Turbulent Dissipation Rate	Least Square Cell-Based Pressure Staggering Option (PRESTO!) Second Order Upwind Compressive Second Order Upwind Second Order Upwind
Solver Configuration	Pressure–Velocity Coupling	Pressure-Implicit with Splitting of Operators (PISO)
Time Step	Number of Time Steps	105 s
	Time Step Size	0.01 s
	Maximum Iterations/Time Step	200
Convergence Criteria	-	Less than 0.001

The separator model was divided into two sections. The top section was gas phase section, and the bottom section was bulk liquid section. From the mesh dependency testing, the gas phase and bulk liquid sections was meshed with sizes of 1.7 mm and 5.5 mm, respectively, to produce results

that were very close to single mesh sizes of 1.5 mm and 1.7 mm. This mesh optimization produced results with a difference of 8%, and the mesh dependency testing results for different mesh sizes are shown in Figure 8. The computational time with the optimized mesh was reduced to 43.75% of initial computational time. The CFD settings for the solver configuration, discretization, and time step settings are listed in Table 2.

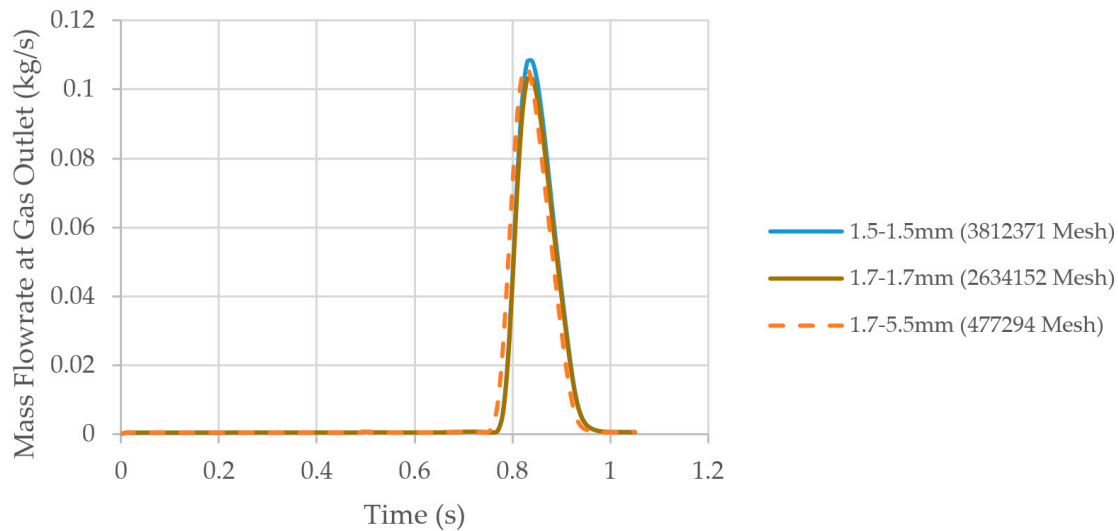


Figure 8. Comparison of selected improved mesh sizes and single meshes of 1.5 and 1.7 mm.

On top of the mesh dependency result, the convergence plot for continuity, x-, y- and z- velocities, k , ϵ , and the volume fraction showed similar trends and iterations of 200 for each time step was sufficient for convergence. The convergence plot is shown in Figure 9.

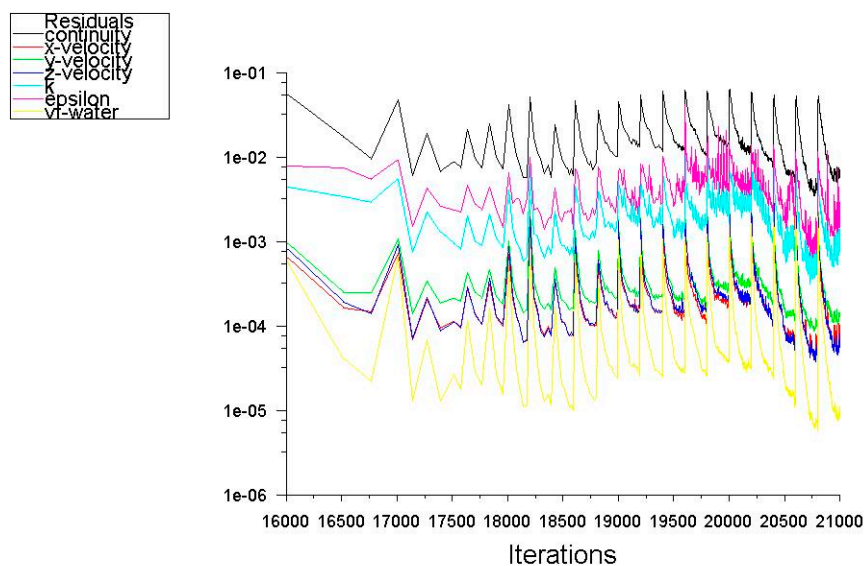


Figure 9. Convergence plots of residuals for separator.

3.1.2. Boundary Conditions

In the CFD simulation for this study, a no-slip wall was used in the model. The model consisted of one inlet and two outlets (one gas-outlet and one liquid-outlet). Mass-flow-inlet boundaries were used at the inlet and liquid-outlet, and at the pressure-outlet boundary for the gas-outlet. On top of the continuity and momentum balance equations, Equation (2) was written as a User-Defined Function (UDF) to describe the mass flow rate of the liquid at the separator inlet. This was done to mimic

the hydraulic jump that was presented in the inlet slug flow and integrated as the liquid flow inlet condition. DEFINE_PROFILE was used in the UDF to describe the mass flow of liquid at separator inlet. The inlet slug flow UDF was important in this CFD simulation, as the hydrodynamics in the separator were greatly dependent on the characteristics of this inlet flow.

$$Q = Ae^{-\frac{(t-\mu)^2}{\sigma}} \quad (2)$$

where Q is the liquid mass flowrate (kg/s), t is time (s), A is the amplitude, μ is the mean, σ is the standard deviation, and e is equal to 2.718.

The mass flow rate of liquid was fitted in a normal distribution equation, known as bell equation as shown in Equation (2). Bell equation was used and verified as a potential model for the inlet mass flowrate for liquid, due to its peak, which can represent a sudden increase in liquid flow (hydraulic jump) at the inlet. The peak of the equation represented the maximum mass flowrate of the liquid fraction at the inlet. Hence, using this new model, the liquid flowrate into the separator will not be constant, but it will be injected as a liquid fraction in the slug flow condition.

The UDF from Equation (2) shall be an equation fitted from the experiment inlet flow. However, the means experiment needs to be carried out to supplement the CFD simulations, and the inlet boundary condition is an empirical fitting. If hydraulic jump behavior can be simulated using a straight pipe, then no experiment will be required. A simulation of the pipe, together with separator, was not in consideration in this study, due to heavy computational and different fluid dynamic profiles between the pipe and the separator which will lead to divergence during the simulation.

There are two methods to validate Equation (2), i.e., half pipe and full pipe models. The half pipe model simplifies the two-phase flow into a single gas phase flow. In this model, only the gas phase is simulated, and the liquid phase was treated as a moving wall at the bottom [14]. However, this model ignored the interaction between the gas and liquid phases, since one phase (liquid phase) was ignored. A full pipe model is preferred, because it simulated both gas and liquid phases, and most importantly, this model took full consideration of interactions between the phases [20]. In our study, a full pipe model was used for the validation of Equation (2), due to its accuracy and reliability.

In a full pipe model, flow pattern simulation was conducted using a straight pipe model with an internal diameter of 7.748 mm. Fluent 19 (ANSYS Inc., Canonsburg, PA, USA) was used to validate the occurrence of the inlet slug flow and the magnitude of the slug flow. The model of the straight pipe with a total length of 100 mm and meshed with the tetrahedron was used in the simulation, and is shown in Figure 10. A mesh dependency was examined on the model, and a mesh size of 0.4 mm with a total number of 647,863 meshes was selected for simulation. The result of the mesh dependency test of the straight pipe is shown in Figure 11, and the CFD settings for the pipe simulation are shown in Table 3. The convergence plot is shown in Figure 12.

Table 3. CFD Setting for the pipe.

Parameter	Description	Value or Settings
Quality of Mesh	Skewness	Max: 0.84995 Average: 0.22238
Discretization Scheme	Gradient Pressure Momentum Volume Fraction Turbulent Kinetic Energy Turbulent Dissipation Rate	Least Square Cell-Based Pressure Staggering Option (PRESTO!) Second Order Upwind Compressive Second Order Upwind Second Order Upwind
Solver Configuration	Pressure-Velocity Coupling	Pressure-Implicit with Splitting of Operators (PISO)
Time Step	Number of Time Steps Time Step Size Maximum Iterations/Time Step	105 s 0.01 s 200
Convergence Criteria	-	Less than 0.001

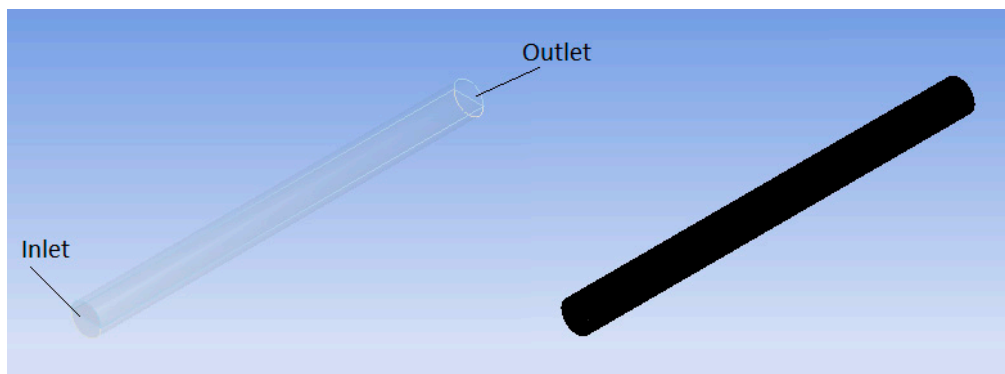


Figure 10. Straight pipe model (left) and straight pipe with mesh (right).

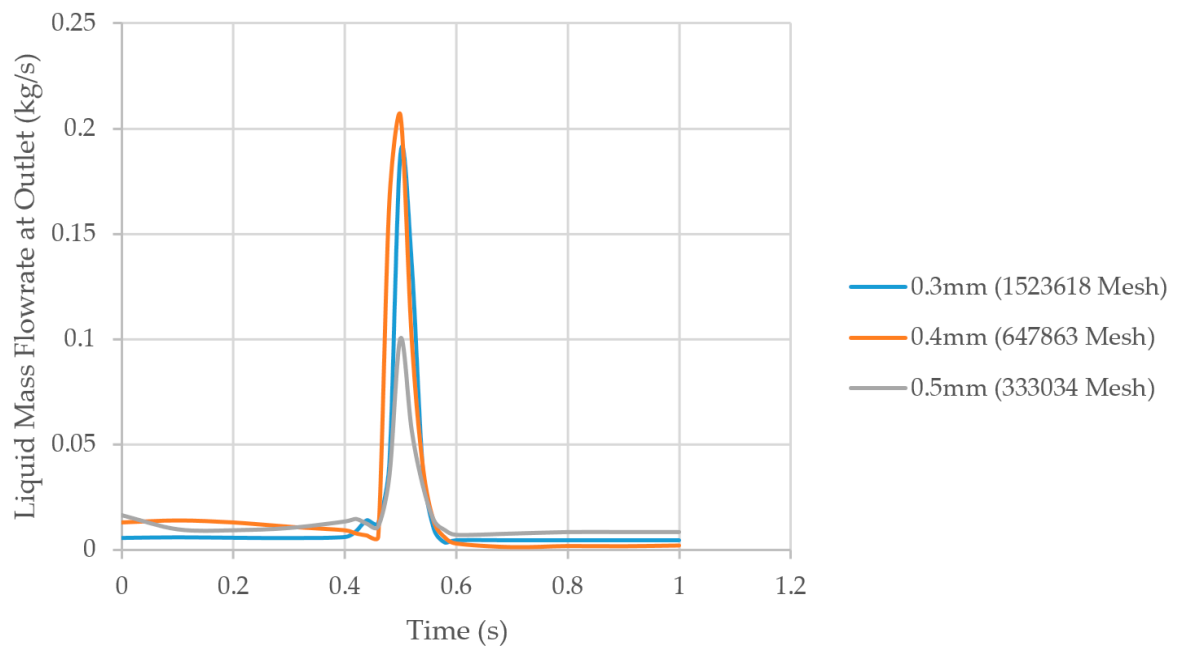


Figure 11. Comparison of different mesh sizes for the pipe.

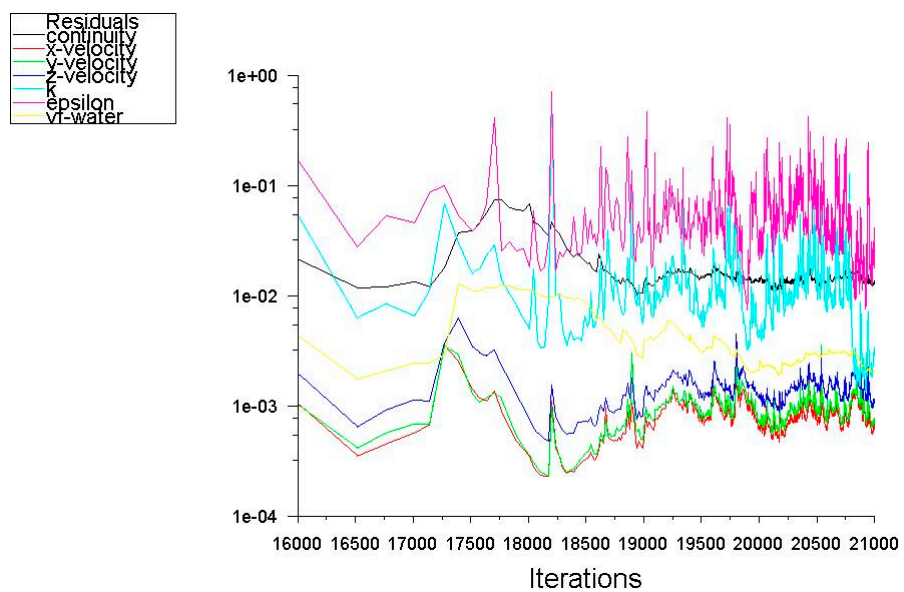


Figure 12. Convergence plot of residuals for the pipe.

The data of the liquid mass flowrate was obtained from the outlet of the full pipe simulation, and Equation (2) was fine-tuned to fit the simulated result before its implementation into the separator inlet boundary condition. However, a criterion of mass conservation must be met by the equation where the integration of the equation from 0 to 1 s equals 0.00702 kg/s, which is the total mass flowrate of the liquid used in the experiment. The normal distribution was generated based on curve fitting, and rewritten as Equation (3) and the curve is illustrated as in Figure 13.

$$Q = 0.1995e^{-\frac{(t-0.5)^2}{0.0000986}} + \frac{0.00702}{2} \quad (3)$$

From Equation (3), the first term on the right represented the peak of the normal distribution curve which was only half of the total liquid mass flowrate, and the other half of the total liquid mass flowrate was evenly distributed, and it was represented in second term on the right.

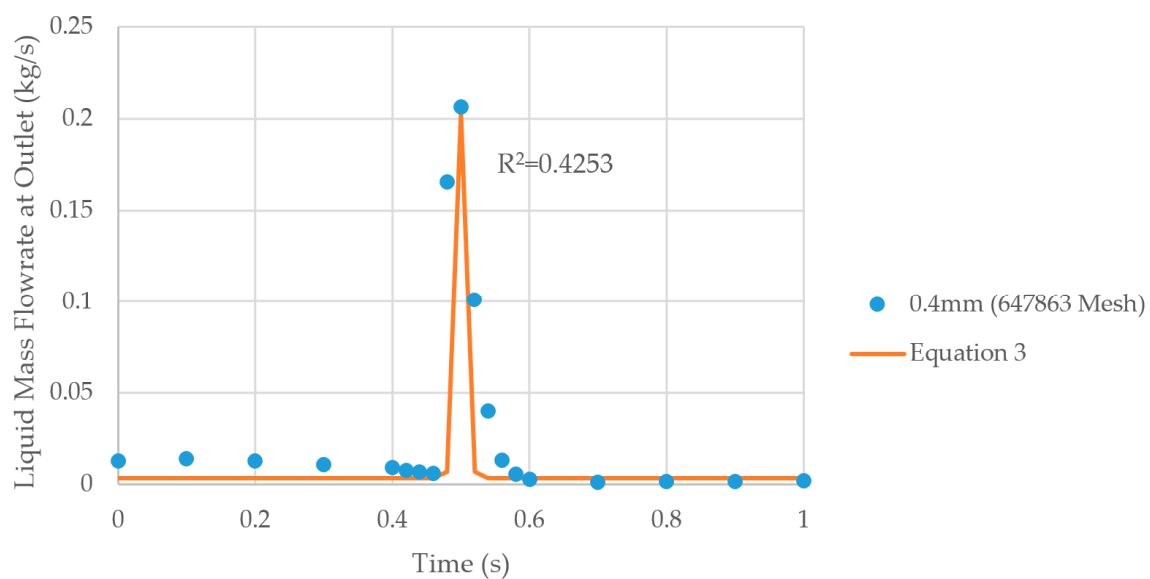


Figure 13. Comparison of ANSYS Fluent data with Equation (3) (normal distribution equation).

The simulated result of the mass flowrate of the liquid at the pipe outlet was compared with those calculated using Equation (3). Both results showed a similar trend, and the peak values were close enough to each other. The simulated peak value was 0.2064 kg/s, while Equation (3) gave 0.2030 kg/s. The results comparison of ANSYS Fluent data and Equation (3) are shown in Figure 13.

Equation (3) was implemented in the simulation as a UDF for the mass flowrate for the liquid inlet for the separator. The equation is simulated the inlet slug flow at the separator inlet, and it improved the simulation result, which subsequently matched the experimental result for all inlet momentums. Figure 14 shows the improvement of the UDF, and a comparison was made for experimental and ANSYS Fluent, with and without the UDF for an inlet momentum of 1000 Pa. Figure 15 shows the inlet slug flow after the implementation of Equation (3) as the UDF for the mass flowrate for the liquid at the inlet, and a comparison is made for all experimental and ANSYS Fluent with UDF. The volume fraction of the liquid phase was patched at a height of 66 mm from the bottom of the vessel at the beginning of the modelling (the same settings, which were used in experimental works). With a combination of mass liquid flowrate from Equation (3) and the mass flowrate of gas, the inlet slug flow at the separator inlet was modelled and validated. The volume and depth of gas pockets generated due to the liquid fraction of inlet slug flow matched well with the experimental results.

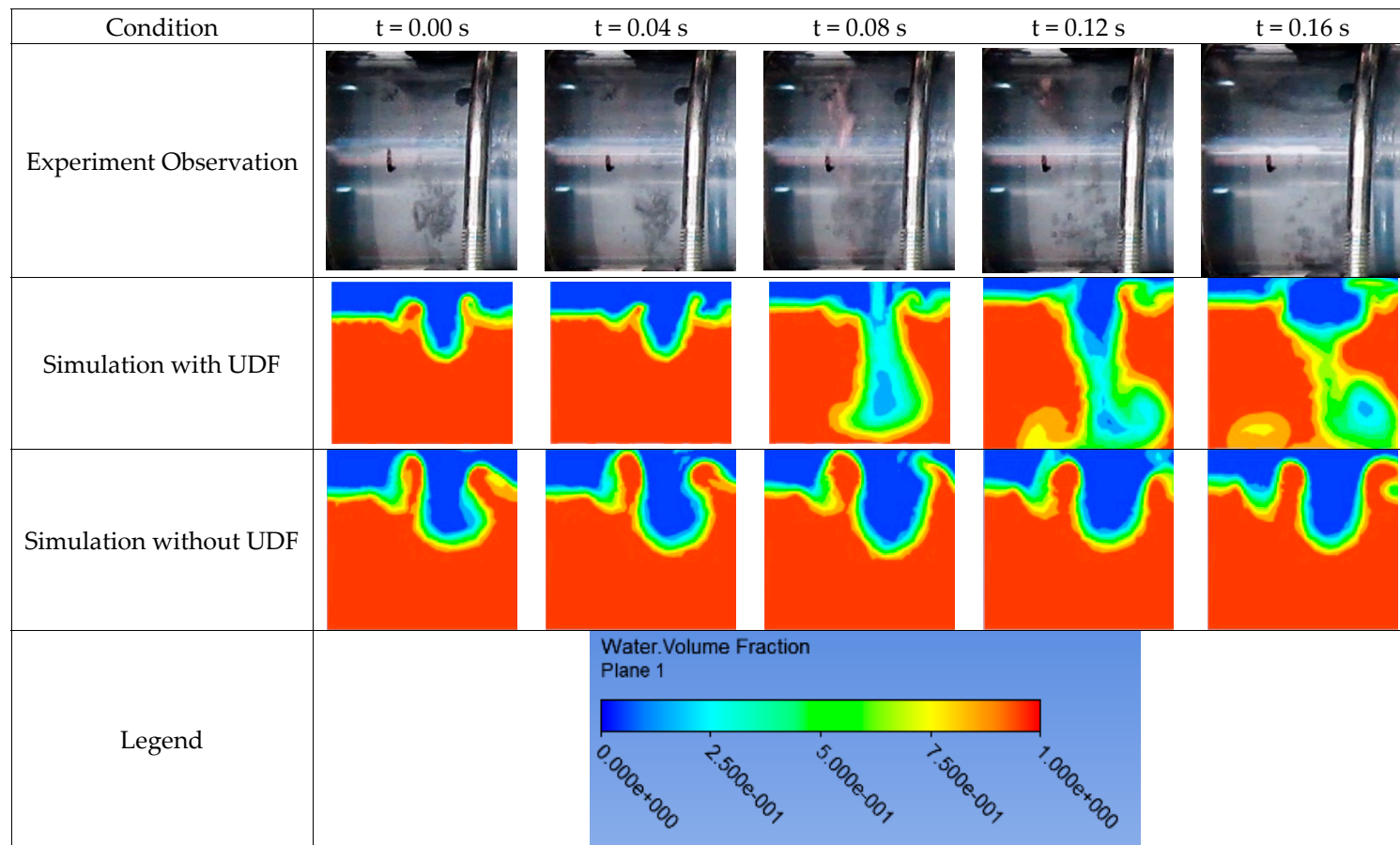


Figure 14. Comparison of experimental observations and volume fractions of water, as simulated by ANSYS Fluent with and without a UDF, at an inlet momentum of 1000 Pa.

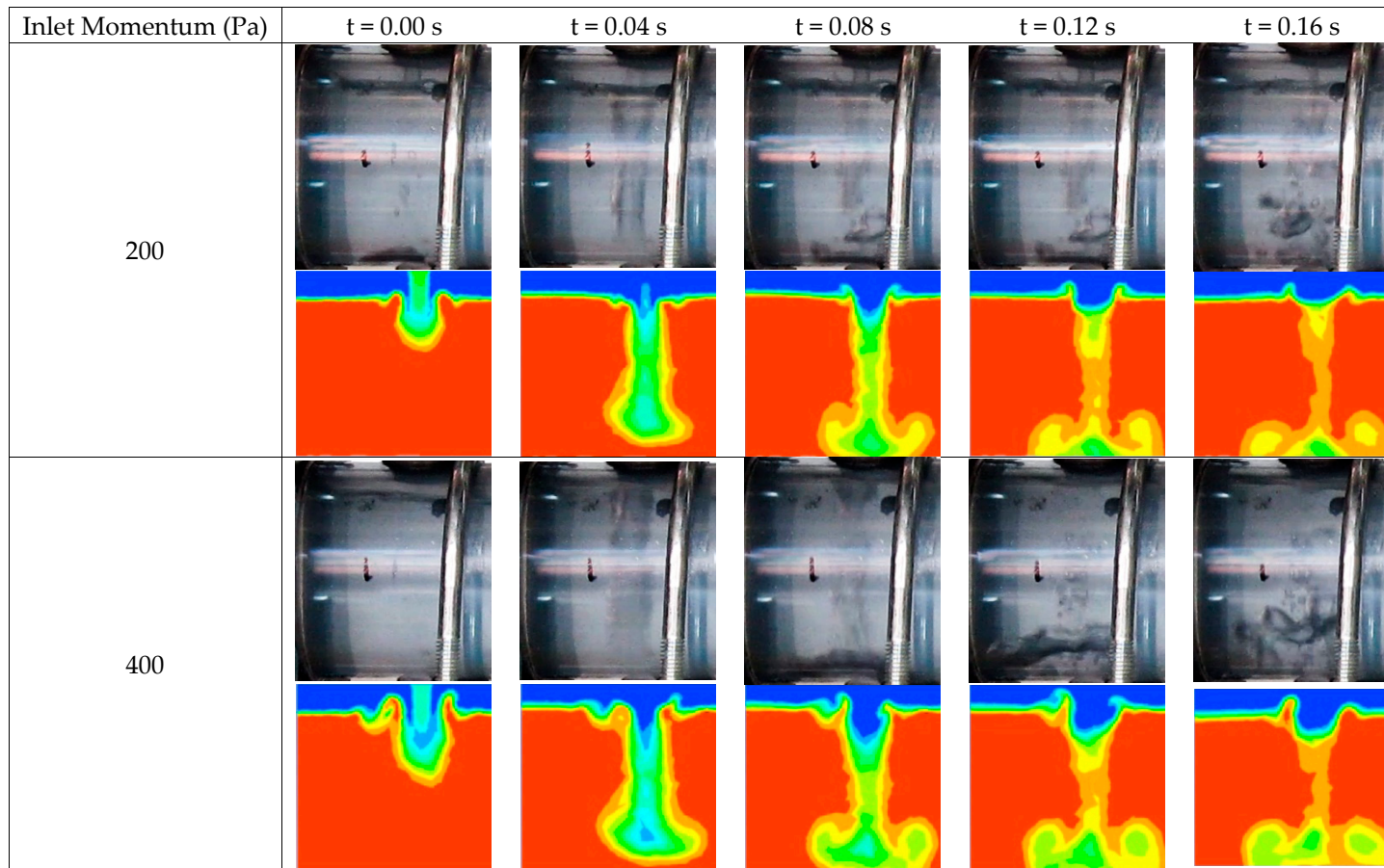


Figure 15. Cont.

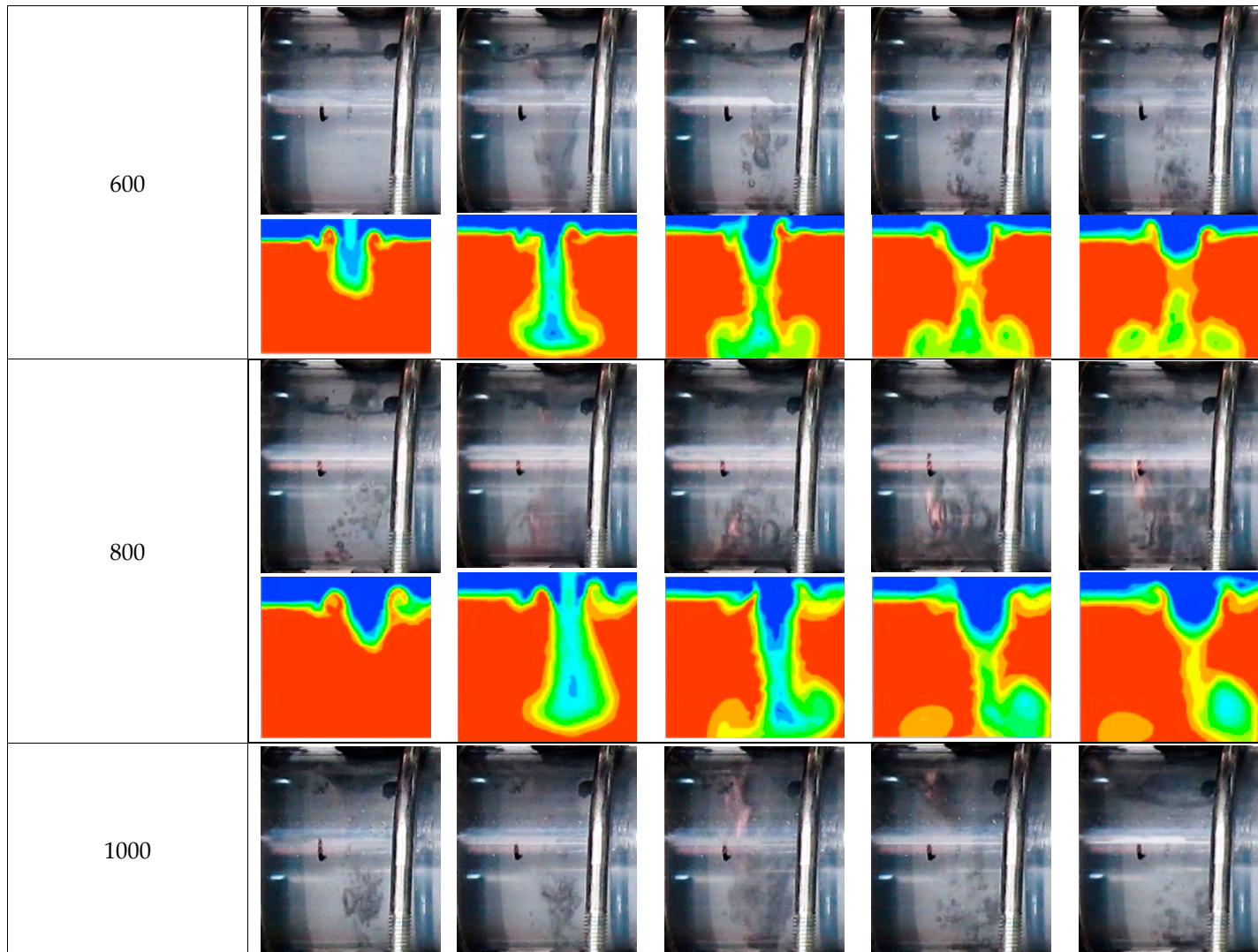


Figure 15. Cont.

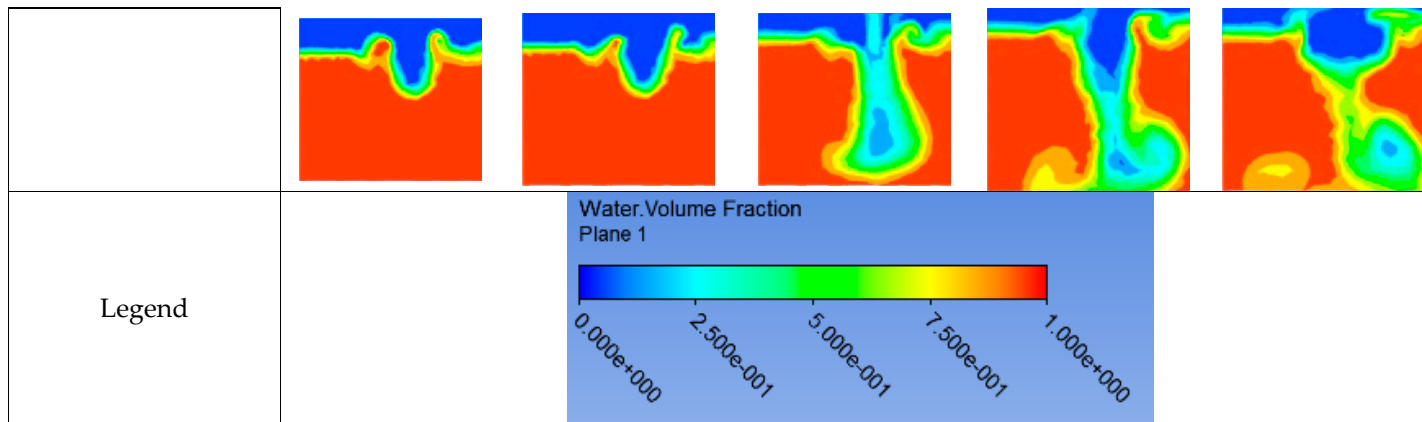


Figure 15. Comparison of experimental and CFD results with integrated UDF.

3.2. Result and Discussion of Computational Fluid Dynamics Work

3.2.1. Cavity Formation

Figure 14 showed the cavity formation at an inlet momentum of 1000 Pa for experimental observation, and CFD simulation with and without UDF integration. From the figure, the CFD-simulated results without the use of UDF has predicted unfavorable cavity formation in the separator where the swallow cavity was formed. The CFD result without the integration of the UDF failed to match with the experimental observation.

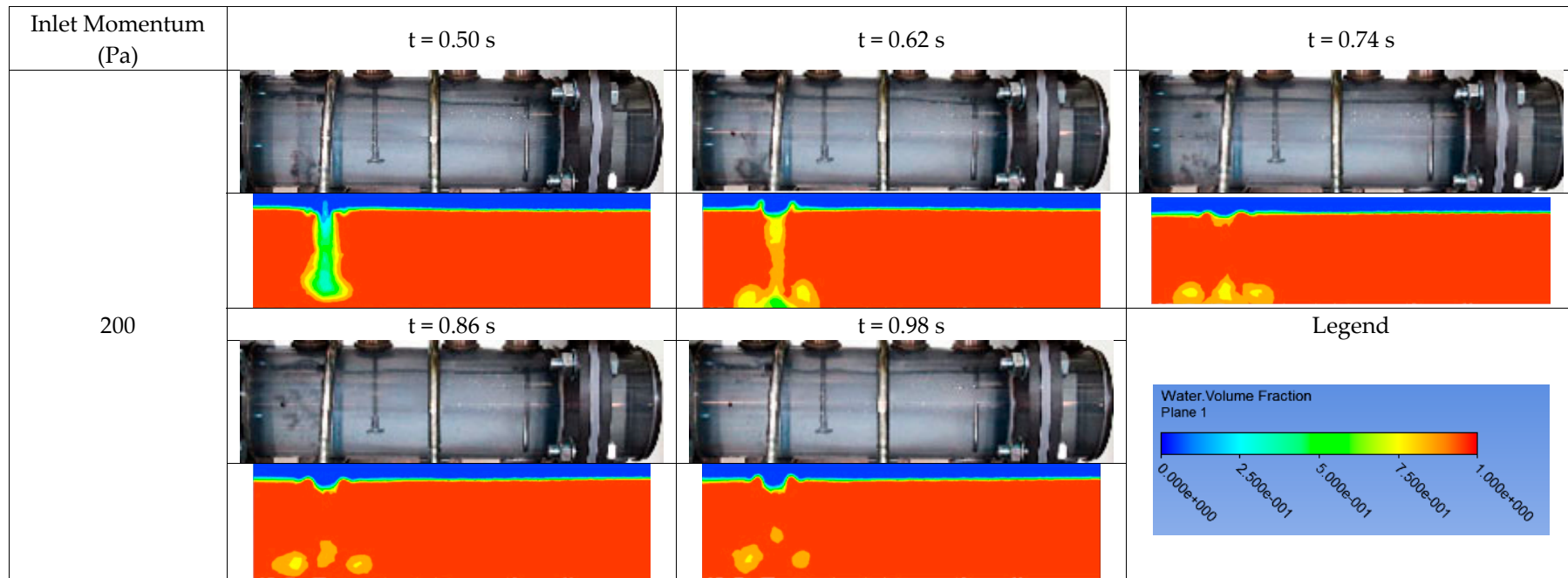
The unsatisfied simulation result was due to the even liquid distribution at the inlet of the separator made in the mass-flow-inlet approach. At the inlet, ANSYS Fluent distributed the liquid volume homogeneously across the surface area of the inlet, and the hydraulic jump was not modelled. Therefore, an improved approach was required to model the hydraulic jump at the inlet for a slug flow. A bell equation was suggested for use in the current work, as explained in the previous section. The bell equation successfully defined the mass flow rate of the liquid at the inlet that mimicked the hydraulic jump, as proven by the cavity formation shown in Figures 14 and 15. The CFD results matched the experimental observation when the UDF that utilized the developed bell equation was integrated into the CFD model simulation. The developed bell equation was one of the important factors that enabled the CFD simulation to predict the hydrodynamics in the separator accurately. The simulation without the UDF might give results that will not be useful for hydrodynamics in the separator.

The similar approach was employed in other CFD simulation, with inlet momentums of 200, 400, 600, 800, and 1000 Pa. Figure 15 shows the comparison for the experimental and CFD results with integrated UDF. The CFD results matched the experiment results, whereby the cavity formation was predicted similar to the experiment observation.

3.2.2. Hydrodynamics in Separator

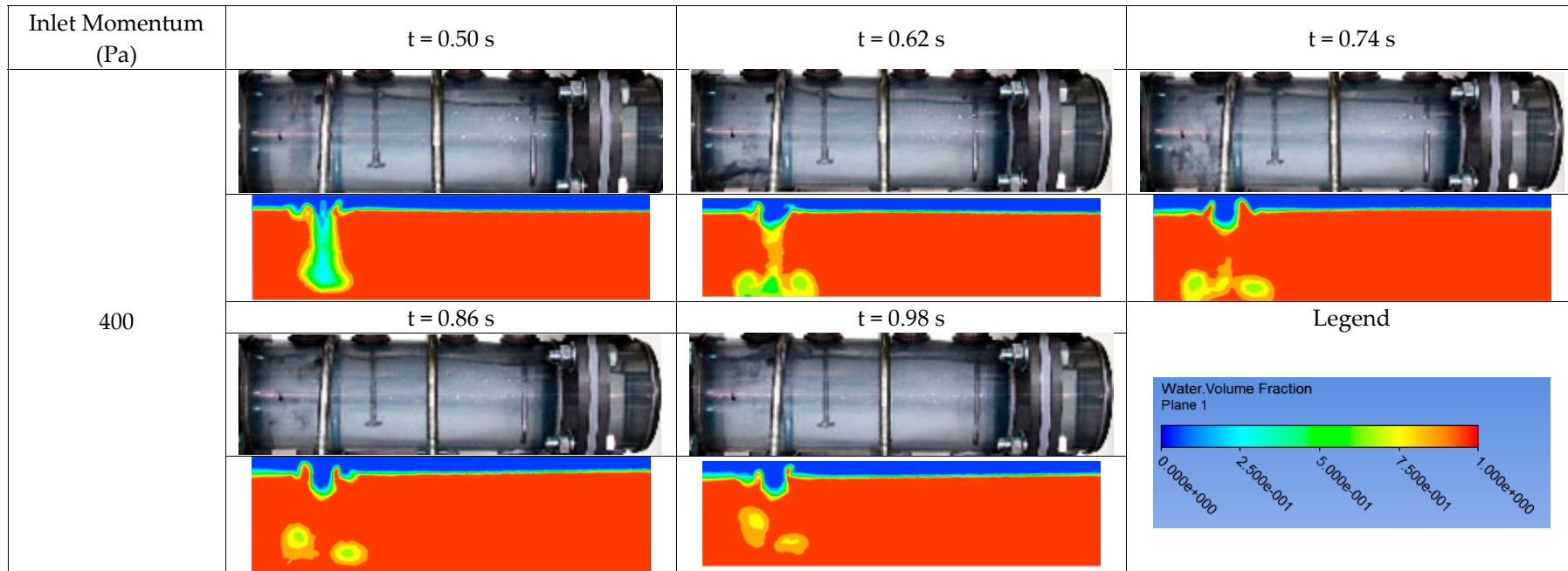
Both simulated and experimental results for hydrodynamics in the separator were shown in Figure 16a–e. It observed that at a higher inlet momentum, the cavity was filled with more gas, and the volume of gas was reduced as the inlet momentum became lower. This has proven the hypothesis that at a lower inlet momentum (200 to 600 Pa), the cavity was filled with a mixture of gas and liquid. At a higher inlet momentum (800 Pa), a stronger cavity was generated after the impact, due to a higher gas volume in the cavity. Both simulated and experiment results well agreed that the sloshing inside the separator was due to a stronger gas pocket being generated, pushing the liquid aside, and subsequently creating a higher intensity wave along the separator length.

The simulated results also showed the same behavior as the physical experiment, where the liquid surface inside the separator was greatly disturbed by the impact of the inlet slug flow. The inlet slug flow created a deep cavity as the liquid jetted from the top of the separator, as shown in Figure 16a–e. The simulation agreed well with experiment data, where at an inlet momentum of 200 to 800 Pa, a wavy stratified flow was generated along the separator after the impact of the inlet slug flow. At 1000 Pa, the impact from the inlet slug flow caused the sloshing inside the separator. Some discrepancy between the experiment and simulation results may have been due to the effect of the control valve in the physical experiment setup, which was not included in the simulation.



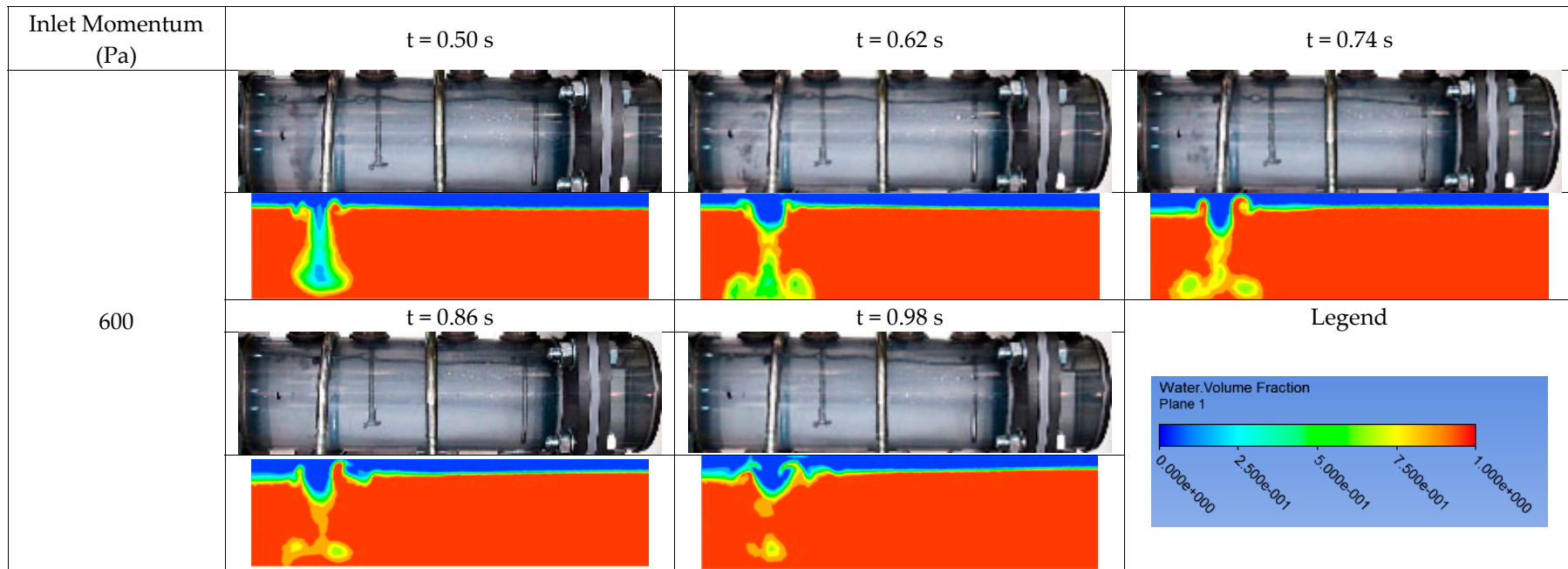
(a)

Figure 16. Cont.



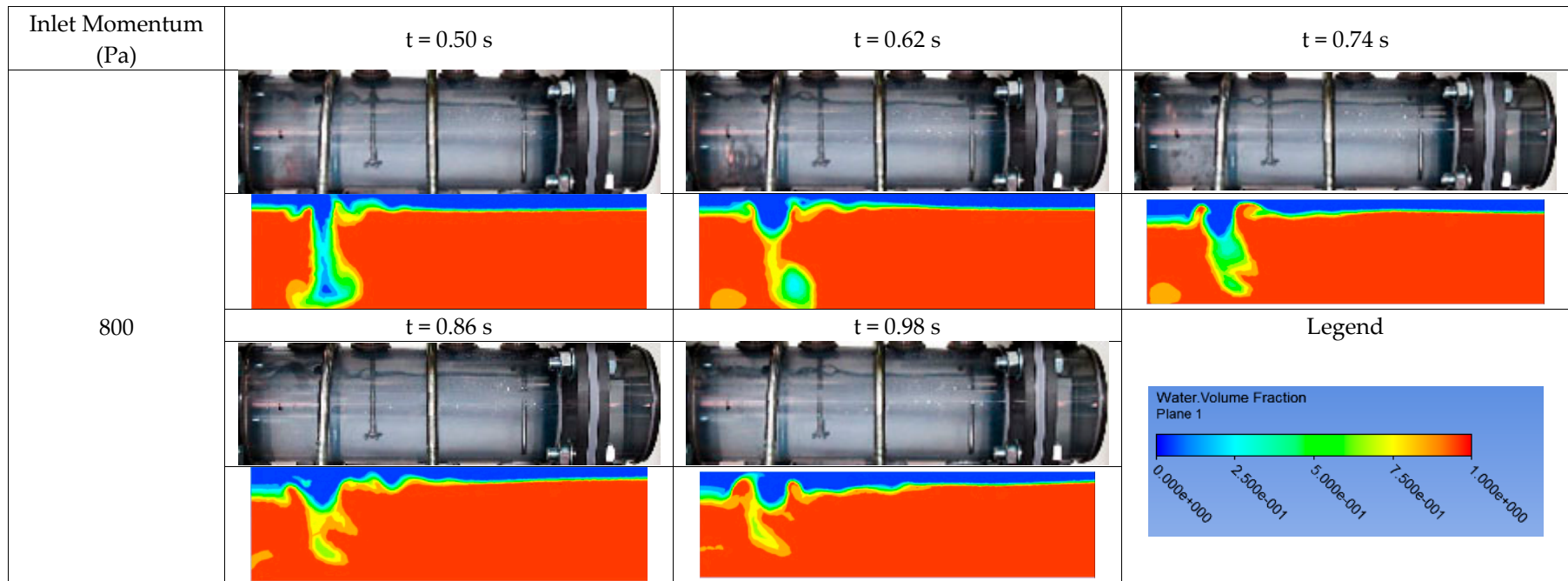
(b)

Figure 16. Cont.



(c)

Figure 16. Cont.



(d)

Figure 16. Cont.

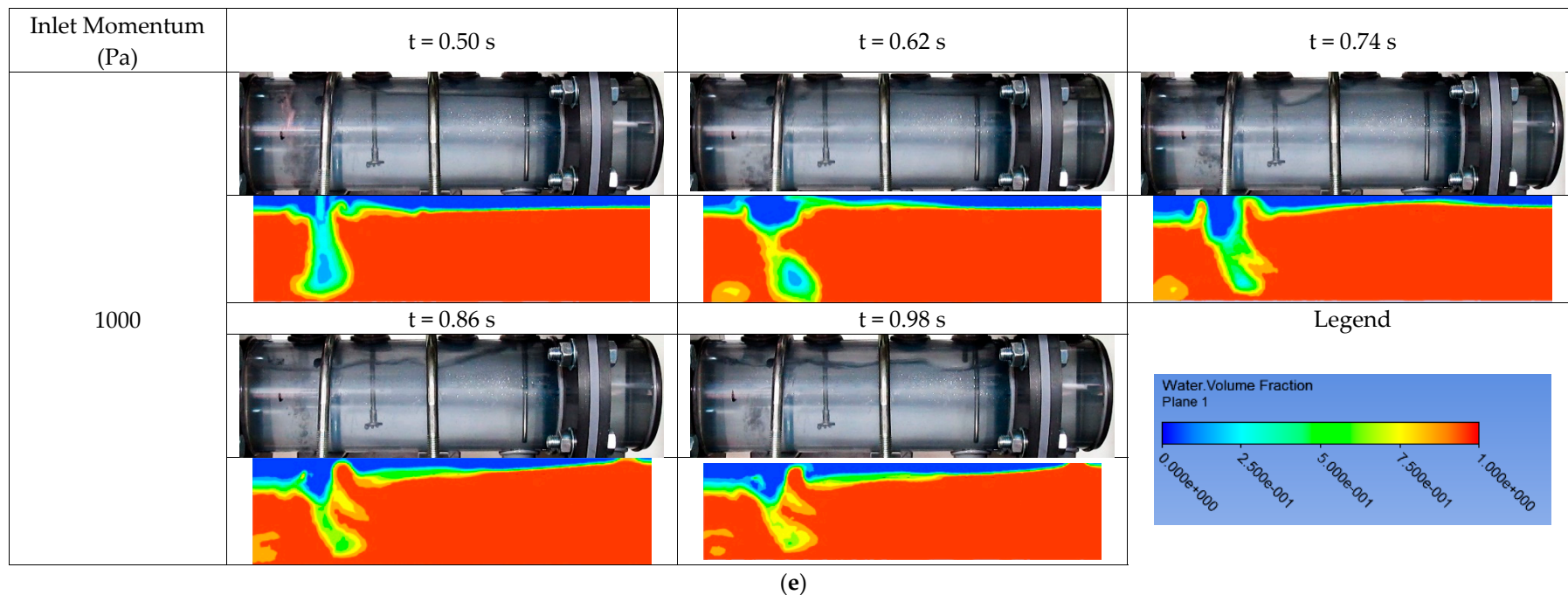


Figure 16. (a) Comparison of both experimental and simulated results for hydrodynamics inside the separator for an inlet momentum of 200 Pa; (b) Comparison of both experimental and simulated results for the hydrodynamics inside the separator for an inlet momentum of 400 Pa; (c) Comparison of both experimental and simulated results for the hydrodynamics inside the separator for an inlet momentum of 600 Pa; (d) Comparison of both experimental and simulated results for the hydrodynamics inside the separator for an inlet momentum of 800 Pa; (e) Comparison of both experimental and simulated results for the hydrodynamics inside the separator for an inlet momentum of 1000 Pa.

3.2.3. Amplification of Inlet Momentum

The inlet slug flow caused severe impact on the separator liquid surface and created a deep cavity during the hydraulic jump. Since the impact of inlet slug flow was not steady, due to the occurrence of hydraulic jump, a transient analysis of a peak flow of inlet momentum using data from CFD simulation was conducted. Amplification of each inlet momentum due to the hydraulic jump are shown in Figure 17.

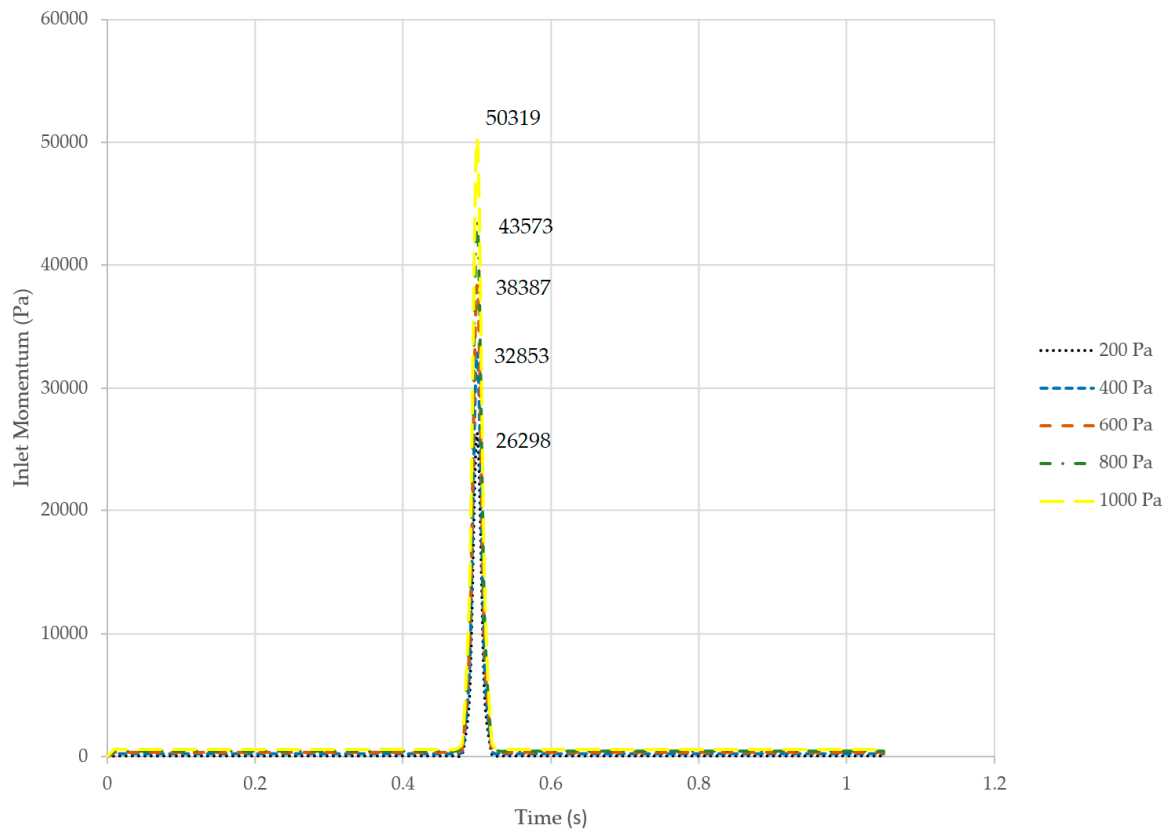


Figure 17. Amplification of inlet momentum due to the liquid slug of the hydraulic jump.

The inlet momentum for 200 to 1000 Pa showed a similar trend where a peak occurred. Before and after the peak, the inlet momentum was relatively low. The peak with a new maximum value indicated that the inlet slug flow amplified the average inlet momentum drastically. The average inlet momentum of 200 Pa was increased to a maximum value of 26,928 Pa, and the inlet momentum of 1000 Pa was increased to a maximum value of 50,319 Pa. The new maximum values for the inlet momentums of 400, 600, and 800 Pa were 32,853, 38,387, and 43,573 Pa, respectively. The cavity created during the impact of inlet slug flow could be explained by the sudden amplification of the inlet momentum to a new high level. This was the main reason behind the formation of a deep cavity and occurrence of sloshing phenomena in the separator.

Table 4 shows the velocity contour in the separator. From Table 4, as the inlet momentum increased, the inlet velocity also increased. The inlet slug flow penetrated deeper and spread wider as the inlet velocity increased. The inlet velocities were increased by the hydraulic jump in the slug flow to a greater extent. At a lower inlet momentum, the velocities increments were more than 100%. The increment velocity for an inlet momentum of 200 Pa was 312.59%, where the highest velocity recorded was 5.90 m/s. The percentage increment of the inlet velocity reduced as the inlet momentum became higher. For inlet momentums of 200, 400, 600, 800, and 1000 Pa, the velocity increments were 312.59%, 167.53%, 115.79%, 85.39%, and 72.21% respectively. The maximum velocities recorded were 5.90 m/s for an inlet momentum of 200 Pa, 7.25 m/s for 400 Pa, 8.61 m/s for 600 Pa, 9.77 m/s for

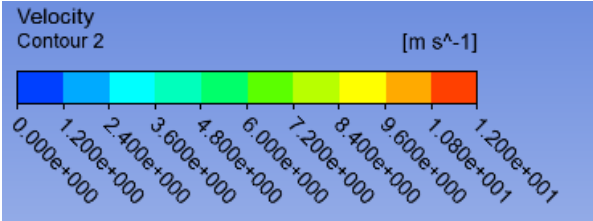
800 Pa, and 11.28 m/s for 1000 Pa. The details of the increment velocity and the velocity contour from ANSYS Fluent are shown in Table 4.

Table 4. Velocity contour of the inlet velocity due to slug flow.

Inlet Momentum (Pa)	Maximum Velocity (m/s)	Average Velocity (m/s)	Maximum Velocity (m/s)
200		1.43	5.90
400		2.71	7.25
600		3.99	8.61
800		5.27	9.77
1000		6.55	11.28

Legend

Velocity Contour 2 [m s⁻¹]



4. Conclusions

This study demonstrated that a deep cavity was formed when the hydraulic jump from the inlet slug flow developed as the inlet hit the liquid surface in the separator. After the impact, liquid turbulence in the separator became rougher as the inlet momentum was higher. Sloshing in the separator did not occur at an inlet momentum of 800 Pa or lower. At an inlet momentum of 1000 Pa, the impact from the hydraulic jump created severe turbulence, and subsequently, sloshing was generated. The occurrence of sloshing upset the separator stability and increased the liquid carryover in the gas phase. This phenomena caused separator to fail to perform, although the separator sized based on state-of-art industrial practices. The sloshing phenomena also explained the reason for high liquid carryover during the inlet slug flow, as observed by other researchers. An extra step to determine the flow pattern in the pipeline transferring the mixture of gas and liquid into the separator is strongly recommended from the outcome of this study, especially for inlet slug flow. A bell equation developed in this study, which integrated as a UDF into the CFD model, was able to simulate the inlet slug flow. With this UDF, the hydrodynamics in the separator was successfully modelled, and it matched the experiment result. The sloshing phenomenon at inlet momentum of 1000 Pa was simulated using this UDF, which was similar to the experimental result. The hydraulic jump in the inlet slug flow was able to amplify the inlet momentum, and the inlet velocity at the inlet could be simulated with the help of CFD. The developed CFD model has provided an alternative method to study the hydrodynamics in the separator, and it is suitable for a stability study of the separator with an inlet slug flow condition. Lastly, the inlet flow pattern is one of the important criteria for separator sizing, on top of inlet momentum and other industrial guidelines. Further study of this criterion and its impact in the separator may leads to better separator performance.

Author Contributions: The project was initiated and supervised by T.S.Y.C. All of the project administration and funding acquisition was carried by T.S.Y.C. The original draft preparation and formal analysis was completed by S.H.L. The experimental methodology was developed by L.C.A., M.A.R., and S.H.L. The simulation methodology was developed by Z.H.B. and S.H.L. The final review and editing of this article was done by T.S.Y.C.

Funding: This research was funded by GERAN UPM grant number [GP-IPS/2017/9539800] and the APC was funded by [GP-IPS/2017/9539800].

Conflicts of Interest: The authors declare no conflict of interest.

Nomenclature

ρ_m	mixture density (kg/m ³)
v_m	mixture mean volume flow velocity (m/s)
Q	liquid mass flowrate (kg/s)
A	amplitude
μ	mean
σ	standard deviation
API	American Petroleum Institute
CFD	Computational Fluid Dynamics
PISO	Pressure-Implicit with Splitting of Operators
PRESTO!	Pressure Staggering Option
PVC	Polyvinyl Chloride
VOF	Volume of Fluid
UDF	User-Defined Function

References

- Katapodis, L. *Oil and Gas Separation Theory, Application and Design*; Society of Petroleum Engineers: Richardson, TX, USA, 1977; pp. 85–89.
- Hansen, E.W.M. Phenomenological Modelling and Simulation of Fluid Flow and Separation Behaviour in Offshore Gravity Separators. *Emerg. Technol. Fluids Struct. Fluid-Struct. Interact.* **2001**, *431*, 23–29.
- Bothamley, M. Gas/Liquid Separator: Quantifying Separation Performance. *Oil Gas Facil.* **2013**, *2*, 21–29. [[CrossRef](#)]
- Chin, R. The Savvy Separator Series: Part 4—The Ghosts of Separators: Past, Present and Future. *Oil Gas Facil.* **2015**, *4*, 18–23.
- Miyoshi, M.; Doty, D.R.; Schmidt, Z. Slug-Catcher Design for Dynamic Slugging in an Offshore Production Facility. *SPE Prod. Eng.* **1988**, *3*, 563–573. [[CrossRef](#)]
- Vallee, C.; Lucas, D.; Beyer, M.; Pietruske, H.; Schutz, P.; Carl, H. Experimental CFD Grade Data for Stratified Two-Phase Flows. *Nuclear Eng. Des.* **2010**, *240*, 2347–2356. [[CrossRef](#)]
- Andreussi, P.; Minervini, A.; Paglianti, A. Mechanistic Model of Slug Flow in Near-Horizontal Pipes. *AIChE J.* **1993**, *39*, 1281–1291. [[CrossRef](#)]
- Bonzanini, A.; Picchi, D.; Ferrari, M.; Poesio, P. Velocity Profiles Description and Shape Factors Inclusion in a Hyperbolic, One-Dimensional, Transient Two-Fluid Model for Stratified and Slug Flow Simulations in Pipes. *Petroleum* **2018**. [[CrossRef](#)]
- Wai, L.L.; Valente, H.; Nguyen, D.T.; Thiam, T.W.; Zhao, Y.; Vivek, K.P. Experimental Study of the Effect of Pressure and Gas Density on the Transition from Stratified to Slug Flow in a Horizontal Pipe. *Int. J. Multiph. Flow* **2016**, *85*, 196–208.
- American Petroleum Institute. *Specification for Oil and Gas Separators*, 8th ed.; American Petroleum Institute: Washington, DC, USA, 2008; p. 14.
- Banks, R.B.; Chandrasekhara, D.V. Experimental Investigation of the Penetration of a High-Velocity Gas Jet Through a Liquid Surface. *J. Fluid Mech.* **1963**, *15*, 13–34. [[CrossRef](#)]
- Cheslak, F.R.; Nicholls, A.J.; Sichel, M. Cavities Formed on Liquid Surfaces by Impinging Gaseous Jets. *J. Fluid Mech.* **1969**, *36*, 55–63. [[CrossRef](#)]
- Mandhane, J.M.; Gregory, G.A.; Aziz, K. A Flow Pattern Map for Gas-Liquid Flow in Horizontal Pipes. *Int. J. Multiph. Flow* **1974**, *1*, 537–553. [[CrossRef](#)]
- Sidi-Ali, K.; Gatignol, R. Interfacial Friction Factor Determination Using CFD Simulations in a Horizontal Stratified Two-Phase Flow. *Chem. Eng. Sci.* **2010**, *65*, 5160–5169. [[CrossRef](#)]
- Lin, S.; Chin, Y.; Wu, C.; Lin, J.; Chen, Y. A Pressure Correction-Volume of Fluid Method for Simulation of Two-Phase Flows. *Int. J. Numer. Methods Fluids* **2012**, *68*, 181–195. [[CrossRef](#)]

16. Park, I.R.; Kim, K.S.; Kim, J.; Van, S.H. A Volume-of-Fluid Method for Incompressible Free Surface Flows. *Int. J. Numer. Methods Fluids* **2009**, *61*, 1331–1362. [[CrossRef](#)]
17. Shih, T.H.; Liou, W.W.; Shabbir, A.; Yang, Z.; Zhu, J. A New $k - \epsilon$ Eddy-Viscosity Model for High Reynolds Number Turbulent Flows—Model Development and Validation. *Comput. Fluids* **1995**, *24*, 227–238. [[CrossRef](#)]
18. Ozan, A.Y.; Yüksel, Y. Simulation of a 3D Submerged Jet Flow Around a Pile. *Ocean Eng.* **2010**, *37*, 819–832. [[CrossRef](#)]
19. Farzad, B.T.; Hamed, Z. Presumed PDF Modeling of a Reactive Two-Phase Flow in a Three Dimensional Jet-Stabilized Model Combustor. *Energy Convers. Manag.* **2010**, *51*, 225–234.
20. Höhne, T.; Hänsch, S. A Droplet Entrainment Model for Horizontal Segregated Flows. *Nuclear Eng. Des.* **2015**, *286*, 18–26. [[CrossRef](#)]



© 2018 by the authors. Licensee MDPI, Basel, Switzerland. This article is an open access article distributed under the terms and conditions of the Creative Commons Attribution (CC BY) license (<http://creativecommons.org/licenses/by/4.0/>).